Geochimica et Cosmochimica Acta 339 (2022) 58–69

Contents lists available at ScienceDirect

Geochimica et Cosmochimica Acta

journal homepage: www.elsevier.com/locate/gca

Mechanism of arsenic release from realgar oxidation in the presence of dissolved oxygen: Effect of reactive oxygen species and light-induced transformation

Lihu Liu [a], Ziwei Zhang [a], Mingzhe Zhang [a], Xiong Yang [a], Chengshuai Liu [b], Guohong Qiu [a,c,*]

[a] Key Laboratory of Arable Land Conservation (Middle and Lower Reaches of Yangtse River), Ministry of Agriculture and Rural Affairs, Hubei Key Laboratory of Soil Environment and Pollution Remediation, College of Resources and Environment, Interdisciplinary Sciences Research Institute, Huazhong Agricultural University, Wuhan 430070, Hubei Province, China

[b] State Key Laboratory of Environmental Geochemistry, Institute of Geochemistry, Chinese Academy of Sciences, Guiyang, 550081, Guizhou Province, China

[c] Shenzhen Branch, Guangdong Laboratory for Lingnan Modern Agriculture, Genome Analysis Laboratory of the Ministry of Agriculture, Agriculture Genomics Institute at Shenzhen, Chinese Academy of Agriculture Science, Shenzhen, China

ARTICLE INFO

Article history:
Received 29 April 2022
Accepted 25 October 2022
Available online 28 October 2022
Associate editor: Mario Villalobos

Keywords:
Arsenic contamination
Realgar
Oxidation
Reactive oxygen species
Sunlight

ABSTRACT

Oxidative dissolution of realgar is an important cause of arsenic (As) pollution in waters and soils. Generally, environmental factors including dissolved oxygen (DO) and solar radiation can lead to the formation of reactive oxygen species (ROS) on As-bearing metal sulfide minerals, which significantly promotes mineral oxidation and As release. Realgar is a typical nonmetallic sulfide mineral with excellent photochemical properties. However, the possible formation mechanism of ROS and the effect of solar radiation on realgar oxidation and the subsequent As release remain elusive. Here, the processes of realgar oxidation and As release were studied under darkness and solar radiation, and the influence of DO and pH on the reaction process was also investigated. The decomposition of H_2O at the sulfur-defect sites and the oxidation of crystal surface As(II) by DO on realgar led to the formation of ROS including H_2O_2 and $^{\cdot}OH$, which play a critical role in realgar oxidation and As release. Under solar radiation, the reactions between electrons and O_2 on light-excited realgar promoted the production of $O_2^{\cdot-}$; while the realgar oxidation and As release could be mainly ascribed to the transformation of realgar to pararealgar in the presence of DO. Under atmospheric conditions, the release ratio of total As in realgar suspension was 4.2% under darkness, and increased to 18.1% under solar radiation. Both higher DO concentration and pH facilitated the generation of ROS and light-induced transformation of realgar to pararealgar, thereby promoting As release. These results imply that the ROS generated on realgar can induce its oxidation and As release in underground aquifers and sediments, and solar radiation may be an important factor causing As pollution in realgar tailings. The findings improve the understanding of As pollution in sulfide mineral mining areas.

1. Introduction

Arsenic (As) is a widely existing toxic chemical element and carcinogen in the environment (Dong et al., 2014; Podgorski and Berg, 2020). Accumulation of As in human body through drinking water and food chain can lead to various chronic diseases and cancers (Li et al., 2016; Tang et al., 2017). Serious As pollution frequently occurs in some countries including the United States, Mexico, Bangladesh, India, Argentina and China (Lengke and Tempel, 2003), and about 190 million people are at risk of drinking water polluted by As around the world (Rodriguez-Lado et al., 2013; Wang et al., 2020). In nature, high contents of As can be found in many sulfide minerals associated with gold and copper, such as arsenopyrite, pyrite, realgar, orpiment and amorphous arsenic sulfide (As_2S_3) (Falteisek et al., 2020; Kerr et al., 2018; Lengke et al., 2009; Qiu et al., 2017). The As released from As-bearing sulfide minerals mainly exists as arsenite (As(III)), which has higher mobility and toxicity relative to arsenate (As(V)) (Liu et al., 2021a; Yu et al., 2007). Therefore, oxidative dissolution of As-bearing sulfide min-

* Corresponding author at: Key Laboratory of Arable Land Conservation (Middle and Lower Reaches of Yangtse River), Ministry of Agriculture and Rural Affairs, Hubei Key Laboratory of Soil Environment and Pollution Remediation, College of Resources and Environment, Interdisciplinary Sciences Research Institute, Huazhong Agricultural University, Wuhan 430070, Hubei Province, China.
E-mail address: qiugh@mail.hzau.edu.cn (G. Qiu).

https://doi.org/10.1016/j.gca.2022.10.037
0016-7037/

eral has become a critical source of As pollution in waters and soils (Kerr et al., 2018; Lengke et al., 2009; Liu et al., 2021a).

Realgar (As_4S_4), a sulfide mineral with an As content of nearly 70 wt.%, is usually found in volcanic eruptions, hot spring deposits and hydrothermal veins (Wu et al., 2017). Realgar is also an important As-bearing mineral in natural shallow aquifer sediments and As-rich wetlands (Drahota et al., 2017; Knappová et al., 2019). High-grade realgar ore can be used in medicine, firecracker and glass industries, and the low-grade realgar ore can be smelted to prepare claudetite (Li et al., 2020; Wu et al., 2017). The As released from realgar generally shows higher mobility compared with that released from As-bearing iron sulfide minerals such as arsenopyrite and pyrite. For example, iron oxyhydroxides/oxides formed during the oxidation of iron sulfide minerals have high affinity for As, which can alleviate the As pollution to a certain extent (Hong et al., 2021; Qiu et al., 2018). As for realgar, due to the lack of iron in its crystal structure, the As(III)/As(V) generated from As (II) oxidation easily pollutes soils, rivers and groundwaters through surface runoff or infiltration (Fan et al., 2018; Wu et al., 2017). Recently, serious As pollution events have been reported in some realgar mining areas of China (Wang et al., 2019). For example, the highest As content in the water exceeds the drinking water limit (10 μg/L) by 2280 times around the realgar mining area in Hechi City, Guangxi province, and that in the paddy soil around the realgar mining area was 9.6 times of the China's national standard (30 mg/kg) in Shimen City, Hunan Province (Wu et al., 2017). The release of As from realgar can be mainly attributed to its oxidation process due to the poor water solubility (Chen et al., 2013). Therefore, elucidation of the process and underlying mechanism of realgar oxidative dissolution and As release can provide important guidance for the prevention and remediation of As pollution in waters and soils (Wu et al., 2017).

Some studies have been focused on the oxidation of realgar by dissolved oxygen (DO) (Langner et al., 2014; Lengke and Tempel, 2005; Renock and Becker, 2010). The results obtained from cyclic voltammetry showed that the oxidation of realgar by DO includes the initial oxidation of realgar to H_3AsO_3 and subsequent oxidation of H_3AsO_3 to H_3AsO_4 under acidic conditions (Lázaro et al., 1997). The total reaction can be summarized as Eq. (1) (Lengke and Tempel, 2003):

$$As_4S_4 + 11O_2 + 10H_2O \rightarrow 4H_3AsO_4 + 4SO_4^{2-} + 8H^+ \quad (1)$$

The intermediate products and reaction rate vary with environmental conditions (Lengke and Tempel, 2005). For example, S(−II) may be oxidized to $S_2O_3^{2-}$, SO_3^{2-} or SO_4^{2-}, and As(II) may be oxidized to As(III) or As(V) (Wu et al., 2017). These studies are mostly about the products and corresponding kinetics of realgar oxidation and attribute As release to the direct oxidation by DO; however, the formation processes of ROS in the process are largely ignored (Lengke and Tempel, 2003; Renock and Becker, 2010; Wu et al., 2017). Generally, sulfide minerals are easily oxidized after contacting with H_2O and air in tailings, which may be accompanied by the production of reactive oxygen species (ROS). As reported, the decomposition of H_2O at sulfur-defect sites on the surface of arsenopyrite and pyrite leads to the production of H_2O_2 and ·OH, thereby promoting the oxidation of these iron sulfide minerals and subsequent As release (Hong et al., 2021; Qiu et al., 2018; Zhang et al., 2016). In the remediation of As pollution in realgar tailings with $FeSO_4$, microwave radiation can result in the generation of more ·OH and $O_2^{\cdot-}$ by promoting the oxidation of $FeSO_4$ by oxygen, which accelerates realgar oxidation (Zhao et al., 2020). However, the possible formation mechanism of ROS and its effect on As release during the oxidation of realgar by DO remain elusive.

The mining processes of sulfide minerals are generally accompanied by soil acidification and acid mine drainage production (Kerr et al., 2018; Kong et al., 2020; Zhang et al., 2016). Chemical neutralization is a widely used remediation method, and the common neutralizers include lime, limestone, sodium hydroxide and magnesium oxide (Naidu et al., 2019). Some previous studies have revealed that an increase in pH can promote As release from realgar tailings (Đorđević et al., 2019; Lengke and Tempel, 2003; Lengke and Tempel, 2005), indicating that simple chemical neutralization may not be very effective in stabilizing realgar tailings. Clarifying the role of ROS in realgar oxidation at different pH values can facilitate the understanding of As pollution and remediation in realgar tailings.

Besides DO and pH, solar radiation also significantly affects the oxidation process of realgar in the environment (Wu et al., 2017). As one of the most important climatic factors, sunlight inevitably affects the migration and transformation of pollutants associated with semiconductor minerals in mine waters, sediments and soils (Doane, 2017; Liu et al., 2021a; Liu et al., 2022a; Lu et al., 2019). Sunlight can induce the transformation of realgar solid to parareal-gar in the air (Kyono et al., 2005; Naumov et al., 2010; Trentelman et al., 1996). Most sulfide minerals are semiconductors with certain photochemical properties (Doane, 2017; Kong et al., 2018). The reaction of hole (h_{vb}^+)/ electron (e_{cb}^-) and H_2O/DO may lead to ROS (·OH and $O_2^{\cdot-}$) formation on sunlit sulfide minerals, which contributes much to the mineral oxidation and As release (Hong et al., 2018; Hong et al., 2020; Hong et al., 2022). The $O_2^{\cdot-}$ produced on light-excited stibnite (Sb_2S_3) can significantly promote Sb release (Hu et al., 2015), and the similar process was also found in the oxidation of amorphous arsenic sulfide (As_2S_3) exposed to visible light (Lu et al., 2019). Realgar has different crystal structure and chemical composition from the amorphous arsenic sulfide (Lengke and Tempel, 2003), which may lead to significant differences in their photochemical process of As release. However, there has been little research on the influence of solar radiation on As release from realgar in tailings.

The present study systematically explored the oxidation and As release processes of realgar under darkness and light radiation, and the influence of DO and pH on the reaction process was also studied. X-ray diffractometer (XRD), X-ray photoelectron spectroscopy (XPS) and field emission scanning electron microscopy (FESEM) were applied to analyze the changes in crystal structure and the valence of As and S during realgar oxidation. The content of dissolved S species was also determined to study the oxidation of S. The possible ROS and their roles in As release were qualitatively and quantitatively detected by electron paramagnetic resonance (EPR) spectroscopy and the addition of scavengers in the reaction system.

2. Materials and methods

2.1. Realgar collection and characterization

Natural realgar ore was collected from the realgar mine located in Luodian County, Qiannan Buyei and Miao Autonomous Prefecture, Guizhou Province, China. The realgar ore was ground through a 200-mesh sieve. In order to study the effect of surface As(III) on realgar oxidation and ROS formation, the realgar powder was treated with HCl solution (1.0 mol/L) for 12 h with the introduction of N_2 (99.99%), and then rinsed with deoxidized deionized water and acetone until the supernatant conductivity was $\leq$ 20 μS/cm. The obtained realgar powder was stored in a vacuum bag without light after vacuum drying.

The realgar powder was dissolved by microwave digestion for the determination of chemical composition. Realgar (0.1 g) was added to the mixed solution of hydrofluoric acid (2 mL), concentrated hydrochloric acid (6 mL) and concentrated nitric acid

(2 mL). The mixed solution was placed in a CEM Mars 6 microwave digester (190 °C, 40 min) after being left at room temperature for 1 h. The relative content (wt.%) of As, S, Fe, Co, Cd and Ni was 68.02%, 30.61%, 0.12%, 0.17%, 0.01% and 0.16%, respectively, as obtained through the determination of their concentration in the digested solution with an inductively coupled plasma-optical emission spectrometer (ICP-OES, Agilent 5110). The molar ratio of As to S was 1:1.05, and the purity of realgar was 98.6%.

2.2. Photochemical reaction of realgar

Most UV (ultraviolet)-A (315–400 nm) and visible light in solar radiation can reach the Earth's surface after penetrating the atmosphere (Liu et al., 2021a). Therefore, the UV LED lamps with the maximum light intensity at 395 nm were employed to simulate sunlight radiation in the laboratory to evaluate its effect on realgar oxidation and As release. The photochemical oxidation experiment of realgar was carried out in a 500-mL quartz bottle with five necks. Two UV LED lamps (220 mm × 185 mm) and a magnetic stirrer were respectively placed on the left, rear and bottom side of the quartz bottle (Fig. S1). The wavelength distribution of the LED lamp has been described in our previous report (Liu et al., 2022b). The light intensity was determined to be 17.0 mW/cm^2 within the band of 375–475 nm at the center of the quartz bottle. During the reaction under darkness, light was avoided by turning off the light sources and wrapping the reaction system with aluminum foil. The temperature difference between the reaction under darkness and UV radiation was less than 3 °C (Fig. S1).

Realgar powder (0.15 g) and deionized water (300 mL) were added into the quartz bottle, and the uniform realgar suspension (0.5 g/L) was obtained by ultrasound for 10 min. NaOH/HCl solution (0.05–1.0 mol/L) was used to adjust the initial pH of the suspension to 5.0. The reaction lasted for 6 h. At 0, 10, 30, 60, 120, 180, 240, 300 and 360 min, suspensions at a volume of 10 mL were taken out and passed through microporous (0.22 μm) membrane to collect the supernatant, and the remaining solids were stored in a vacuum bag without light after washing with deoxidized deionized water and vacuum drying.

The experiments were respectively conducted under oxic and anoxic conditions with the continuous introduction of air and N_2 (99.99%). The initial concentration of dissolved oxygen ([DO]) in the suspension was 0.7 and 6.4 mg/L with the introduction of N_2 and air, respectively. The effect of pH was investigated at pH 2.0 and 8.0. The experiment under atmospheric conditions was also performed outdoors to reveal the influence of actual solar radiation on realgar oxidation and As release at 10:00–16:00 on April 10, 2022. The light intensities within bands of 320–400 nm and 400–1000 nm were 2.5 and 57.0 mW/cm^2, respectively, at 12:00. Each experiment was performed in triplicate.

2.3. Analysis methods

The [DO] and pH were monitored by a DO detector (Inesa, JPB-607A) and a pH detector (Mettler Toledo FE28), respectively. The redox potential (Eh) of the reaction was determined in a two-electrode system on a CHI 660E workstation. A platinum foil and a saturated calomel electrode (SCE) were used as working and reference electrode, respectively. The molybdenum blue method has been widely validated and used to determine the concentration of inorganic As including As(III) and As(V) in aqueous solutions (Hu et al., 2012; Lenoble, 2003; Najafi and Hashemi, 2019; Oscarson et al., 1980). A UV–vis spectrophotometer (Mapada UV-1800) was applied to determine As(V) concentration ([As(V)]) in solutions with the molybdenum blue method at 880 nm (Oscarson et al., 1980; Qiu et al., 2017). The [As(T)] (total As concentration) in solutions was measured after oxidation of dissolved As(III) to As(V) with potassium iodate, and the As(III) concentration ([As(III)]) in solutions was obtained by subtracting the [As(V)] from [As(T)] (Oscarson et al., 1980; Qiu et al., 2017). The detection limits were 0.1 and 0.3 μmol/L for [As(V)] and [As(T)], respectively, as obtained through eleven repeated measurements of reagent blank. As(T) release ratio represents the ratio of As(T) dissolved in solution to that (4539.5 μmol/L) in the pristine realgar. The concentrations of $S_2O_3^{2-}$ ([$S_2O_3^{2-}$]), SO_3^{2-} ([SO_3^{2-}]) and SO_4^{2-} ([SO_4^{2-}]) were analyzed on an ion chromatograph (Dionex ICS-1100) using an AS22 chromatographic column with the mixture of $NaHCO_3$ (1.4 mmol/L) and $NaCO_3$ (4.5 mmol/L) as the eluent (Hong et al., 2018). During the analysis of dissolved sulfide concentration ([S^{2-}]), the solution was immediately added to zinc acetate solution to precipitate S^{2-} from polysulfide, H_2S and HS^- species, and then the ZnS was determined with the methylene blue method on a UV–vis spectrophotometer (Mapada UV-1800) at 650 nm (Wang et al., 2022). The detection limit was 2.2 μmol/L, as obtained through eleven repeated measurements of reagent blank. The possible ROS and S vacancy were detected by EPR (Bruker A300). During the determination of ·OH, reaction suspension (1 mL) was taken out and mixed with 5,5-dimethyl-1-pyrroline *N*-oxide (DMPO, 10 μL) in a centrifuge tube, and then the solution was immediately transferred to a quartz capillary. The EPR signal was recorded by a Bruker A300 spectrometer at room temperature. Methanol was used as the solvent during the determination of $O_2^{\cdot-}$, and the detection of S vacancy was performed under darkness. Superoxide dismutase (SOD, 50 mg/L), peroxidase (POD, 150 mg/L) and sodium benzoate (BA, 10 mmol/L) were respectively added to the reaction system as the scavenger of $O_2^{\cdot-}$, H_2O_2 and ·OH (Kong et al., 2015; Liu et al., 2018; Shu et al., 2019). The determination of *p*-hydroxybenzoic acid was conducted on an Agilent 1200 high performance liquid chromatography at 255 nm, and the concentration of cumulative [·OH] was 5.87 times of *p*-hydroxybenzoic acid (Hong et al., 2018). The instant H_2O_2 concentration ([H_2O_2]) was obtained on the UV–vis spectrophotometer at 551 nm through a *N,N*-diethyl-*p*-phenylenediamine method (Hong et al., 2021).

A Shimadzu 6100 XRD (Cu Kα) was employed to characterize the crystalline phase of realgar at scan rate of 1°/min, operation current of 30 mA and voltage of 40 kV. The band structure of realgar was analyzed through XPS valence band (VB) spectra, Mott–Schottky plot and UV–vis diffuse reflectance spectra (DRS) (Xu et al., 2021). Mott–Schottky characterization was conducted in 0.5 mol/L Na_2SO_4 solution using a three-electrode system on a CHI 660E workstation at a frequency of 1000 Hz. The working electrode was prepared by coating the mixture of 90 wt.% realgar and 10 wt.% polyvinylidene fluoride (adhesive) on an ITO conducting glass with a dimension of 1 cm × 2 cm. A SCE and a platinum foil were used as reference and counter electrode, respectively. The detailed calculation method of the band structure is shown in the supplementary information (supplementary text). A UV–vis spectrophotometer (Purkinje T9) was applied to record the diffuse reflectance spectra (DRS) with $BaSO_4$ as the reference and a scan interval of 1 nm from 400 to 800 nm. The species of As, S and O were determined by XPS (VG Multilab2000, Al Ka, 1486 eV) with charge correction at 284.8 eV. During the fitting of XPS spectra, the As $3d_{(5/2)}$ spectra were fitted with three double peaks of As (II), As(III) and As(V). The double peak interval was 0.7 eV, and the peak area of the companion peak was two-thirds that of the main peak (Zhao et al., 2020). The S $2p_{(3/2)}$ spectra were fitted with three double peaks of sulfide (S^{2-}), polysulfide (S_n^{2-}) and elemental sulfur (S^0). The double peak interval was 1.2 eV, and the peak area of the companion peak was half that of the main peak (Fan et al., 2018; Hong et al., 2021). Three peaks of O^{2-}, –OH and H_2O were included in the fitting of O 1s spectra (Liu et al., 2021a). The uncertainties were obtained by three times of fitting with varying background positions (Ilton et al., 2016). The micromorphology and

element distribution of the samples were analyzed by FESEM (Tescan MIRA4) equipped with an energy dispersive X-ray (EDX) spectrometer.

3. Results

3.1. Realgar oxidation and As release

The effects of UV radiation from sunlight on realgar oxidation and As release were investigated at initial pH 5.0 and under oxic conditions (Fig. 1). Under darkness, the As released into the solution was mainly As(III), and the [As(III)] increased with reaction, reaching 161.8 μmol/L after 6 h; besides, the [As(T)] was 190.6 μmol/L with an As(T) release ratio of 4.2%. Under UV radiation, As(III) was also the main dissolved As species. Compared with that under darkness, the final [As(V)] decreased from 28.8 to 15.5 μmol/L, accompanied by increases in final [As(III)] and [As (T)]. At 6 h, the [As(T)] and [As(III)] reached 770.3 and 754.8 μmol/L, respectively, with the As(T) release ratio increasing to 17.0%. SO_3^{2-} was not detected under both darkness and UV radiation, while [$S_2O_3^{2-}$] and [SO_4^{2-}] gradually increased and [S^{2-}] increased first and then decreased with reaction time, with $S_2O_3^{2-}$ being the dominant species of dissolved S. At 6 h, the [S^{2-}], [$S_2O_3^{2-}$] and [SO_4^{2-}] were 3.3, 55.8 and 47.3 μmol/L under darkness, and 10.3, 231.3 and 129.0 μmol/L under UV radiation, respectively. The above results indicated that UV radiation can significantly promote realgar oxidation and the subsequent release of As.

3.2. ROS production from realgar oxidation

The ROS in the above reaction system were qualitatively analyzed by EPR spectra (Fig. 2a and b). DMPO-·OH signal was detected at the initial stage as well as at 10 min under darkness and UV radiation, whose intensity was higher under UV radiation. DMPO-$O_2^{\cdot-}$ signal was not detected at the initial stage and at 10 min under darkness, but detected at 10 min under UV radiation (Liu et al., 2022b; Lu et al., 2019), indicating the formation of more ·OH and $O_2^{\cdot-}$ under UV radiation. Fig. 2c and d present the instant [H_2O_2] and cumulative [·OH]. Under darkness, the instant [H_2O_2] increased with reaction time, reaching 6.7 μmol/L at 6 h; while the instant [H_2O_2] under UV radiation was lower than that under darkness, and first increased and then decreased with reaction time, with a maximum of 1.7 μmol/L at 15 min. The cumulative [·OH] increased with reaction time, and reached 6.7 and 3.7 μmol/L at 6 h under darkness and UV radiation, respectively. Further, BA, SOD and POD were introduced to the suspension to capture ·OH, $O_2^{\cdot-}$ and H_2O_2, respectively (Fig. 2e and f). Under darkness, the addition of SOD caused a slight decrease in the [As(T)], while the addition of BA and POD significantly inhibited As release. After 6 h of reaction, the presence of BA, SOD and POD reduced the [As(T)] from 190.6 μmol/L to 132.5, 158.3 and 114.1 μmol/L, respectively. Under UV radiation, BA and SOD also inhibited As release, while POD exhibited little effect on the [As(T)]. After 6 h of reaction, BA and SOD decreased the [As(T)] from 770.3 μmol/L to 574.9 and 642.1 μmol/L, respectively.

3.3. Crystalline phase changes of realgar

The crystalline phase of the solid products was characterized with XRD after reaction (Fig. 3a). Only the diffraction peaks of realgar (PDF, 41-1494) were found in the XRD pattern of the initial sample, which was consistent with the previous report (Wang et al., 2022). The diffraction peak of elemental S (PDF, 34-0941) occurred under darkness. Pararealgar (PDF, 33-0127) and elemen-

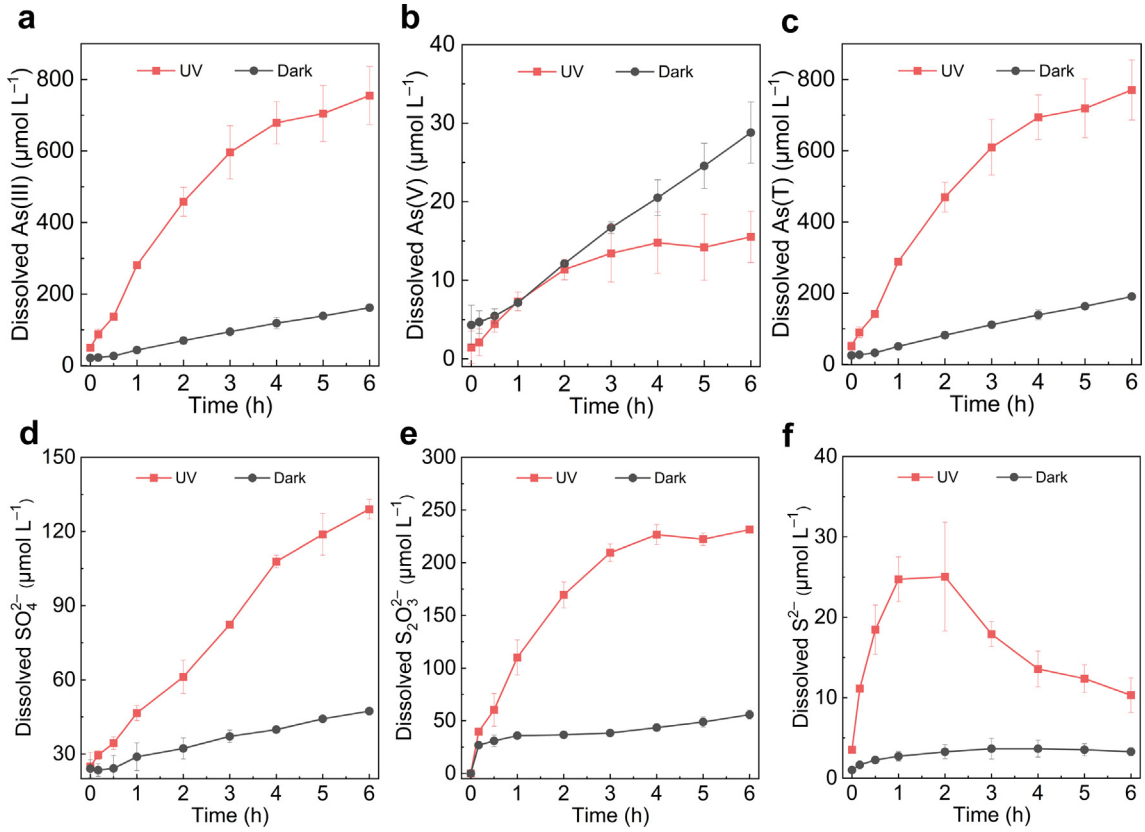

Fig. 1. Dissolved [As(III)] (a), [As(V)] (b), [As(T)] (c), [SO_4^{2-}] (d), [$S_2O_3^{2-}$] (e) and [S^{2-}] (f) in realgar suspension (0.5 g/L) under darkness and UV radiation at initial pH 5.0 and oxic condition.

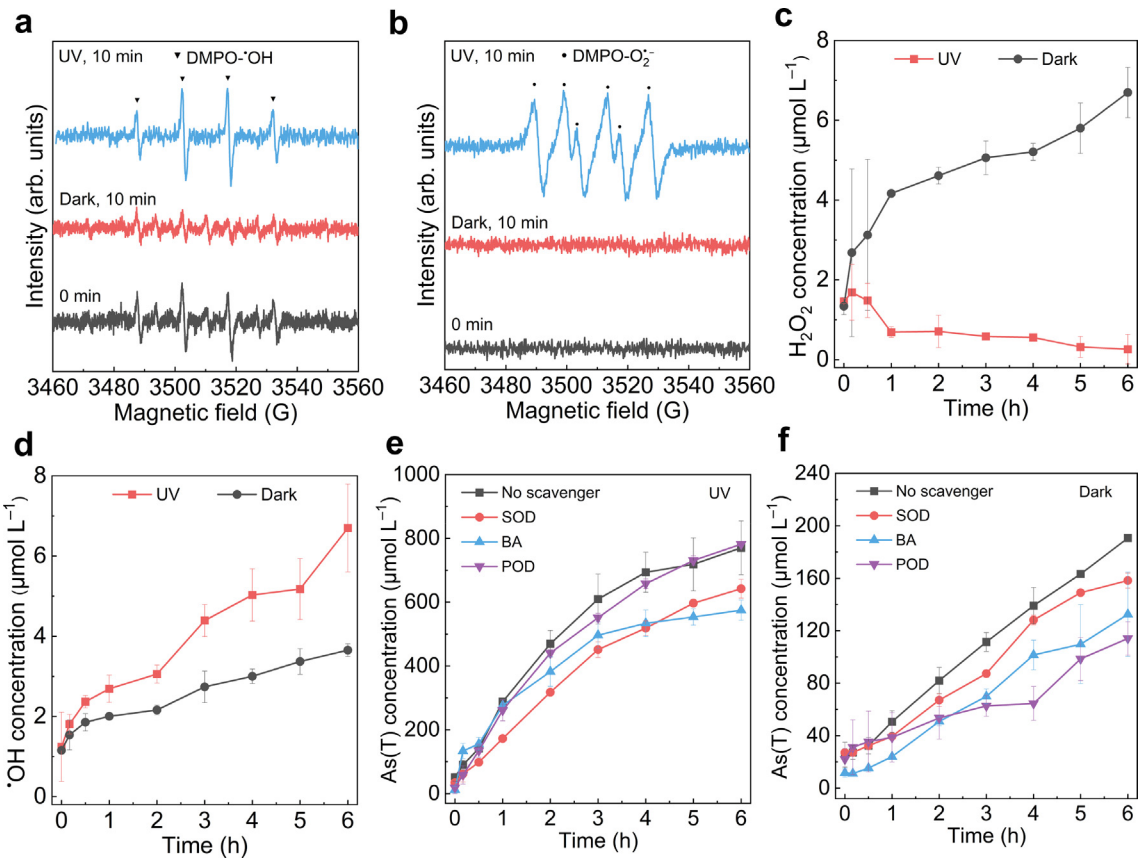

Fig. 2. EPR spectra of DMPO-·OH (a), DMPO-$O_2^{\cdot-}$ (b) and instantaneous [H_2O_2] (c), cumulative [·OH] (d) and [As(T)] after the addition of scavengers (e, f) in realgar suspension (0.5 g/L) under darkness and UV radiation at initial pH 5.0 and oxic condition.

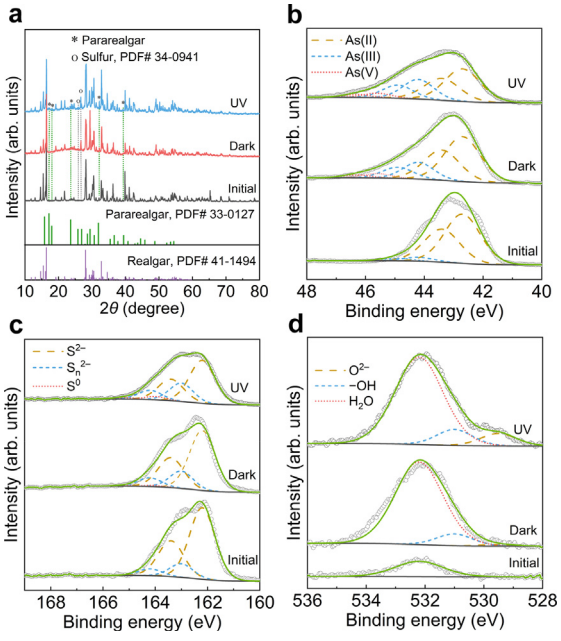

Fig. 3. XRD patterns (a), XPS As $3d_{(5/2)}$ (b), XPS S $2p_{(3/2)}$ (c) and XPS O 1s (d) spectra (open circles) and corresponding fitting spectra (yellow green lines) of realgar before and after reaction under darkness and UV radiation at initial pH 5.0 and oxic condition.

tal S were formed under UV radiation. The species of As, S and O were further characterized by XPS (Fig. 3b–d), and the fitting results are shown in Table 1. In the As $3d_{(5/2)}$ spectra, 42.7, 44.2 and 45.6 eV correspond to the binding energy of the main peak for As(II), As(III) and As(V), respectively (Zhao et al., 2020). In the S $2p_{(3/2)}$ spectra, 162.2, 163.0, 164.0 and 168.4 eV represent the binding energy of the main peak for S^{2-}, S_n^{2-}, S^0 and SO_4^{2-}, respectively (Fan et al., 2018; Hong et al., 2021). No SO_4^{2-} peak was found in the XPS spectra, which was consistent with the previous research about the oxidation of pure realgar and As_2S_3 by DO (Fan et al., 2018; Lu et al., 2019). This phenomenon may be ascribed to the weak adsorption ability of realgar for SO_4^{2-}. The isothermal adsorption of realgar for SO_4^{2-} was not conducted due to the obvious oxidation of realgar even at low [DO]. Therefore, only S^{2-}, S_n^{2-} and S^0 were included in the fitting of S $2p_{(3/2)}$ spectra. In the O 1s spectra, 529.5, 531.0 and 532.2 eV are ascribed to the binding energy of O^{2-}, −OH and H_2O, respectively (Liu et al., 2021a). The presence of As(III), S_n^{2-} and O^{2-} indicated the oxidation of a small part of initial realgar. After reaction, the increase in the relative content of As(III), As(V), S_n^{2-}, S^0, O^{2-} and −OH and decrease in that of As(II), S^{2-} and H_2O indicated the oxidation of realgar under darkness, which was further promoted by UV radiation.

3.4. Micromorphology changes of realgar

Changes in the micromorphology and chemical composition of realgar were analyzed by FESEM-EDX (Fig. 4). A flake-like micromorphology was observed with a few irregular crystal particles on the surface of initial realgar. The relative contents (at.%) of As, S and O were 48.2%, 45.5% and 6.3%, respectively. The molar ratio of As to S was 1.06, which was in agreement with the result of chemical analysis (1.05). As, S and O were evenly distributed on realgar surface, and no obvious difference was observed among the As, S and O maps after reaction under darkness and UV radia-

Table 1
Relative contents of As, S and O species obtained from the fitting of XPS spectra of realgar before and after reaction under darkness and UV radiation at initial pH 5.0 and oxic condition. Uncertainties were obtained by three times of fitting with varying background positions.

Species		Binding energy (eV)	Full width at half aximum (FWHM)	Relative content (at.%)		
				Initial	Dark	UV
As	As(II)	42.7	1.5	92.7 ± 1.0	72.1 ± 0.8	60.5 ± 0.7
		43.4	1.5			
	As(III)	44.2	1.3	7.3 ± 1.0	22.8 ± 0.2	31.6 ± 0.3
		44.9	1.3			
	As(V)	45.6	1.2	0	5.1 ± 0.6	7.9 ± 1.0
		46.3	1.2			
S	S^{2-}	162.2	1.2	85.5 ± 0.4	76.9 ± 2.1	68.7 ± 0.9
		163.4	1.2			
	S_n^{2-}	163.0	1.1	14.5 ± 0.4	22.3 ± 2.8	27.0 ± 1.1
		164.2	1.1			
	S^0	164.0	1.0	0	0.7 ± 0.6	4.3 ± 0.2
		165.2	1.0			
O	O^{2-}	529.5	1.5	0.4 ± 0.1	1.2 ± 0.3	8.8 ± 0.5
	−OH	531.0	1.5	0	9.7 ± 0.4	11.4 ± 0.3
	H_2O	532.2	2.0	99.6 ± 0.1	89.1 ± 0.3	79.8 ± 0.5

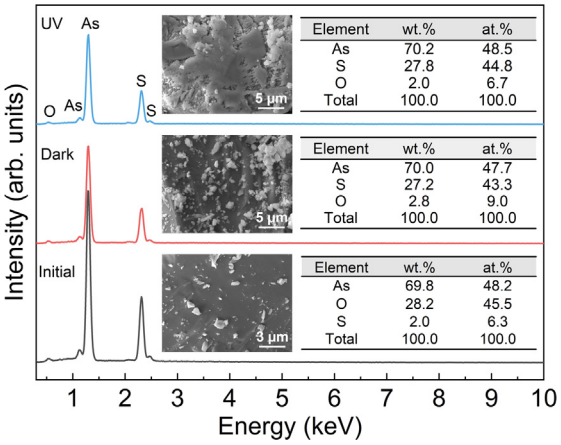

Fig. 4. FESEM images and EDX analysis of initial realgar and realgar after reaction under darkness and UV radiation at initial pH 5.0 and oxic condition.

tion (Fig. S2). Under darkness, more irregular crystal particles were observed, and the relative contents of As, S and O became 47.7%, 43.3% and 9.0%, respectively. Under UV radiation, the flake structure was broken, resulting in the appearance of more irregular crystal particles, and the relative contents of As, S and O were 48.5%, 44.8% and 6.7%, respectively. These results further indicated the occurrence of more obvious weathering of realgar under UV radiation.

3.5. Influence of dissolved oxygen on As release and ROS production

The oxidation of sulfide minerals and formation of ROS are significantly affected by DO (Hong et al., 2021; Lengke and Tempel, 2003). The reactions were performed under anoxic conditions to examine the influence of DO on realgar oxidation and As release (Fig. 5). As shown in Fig. S3, the [DO] in the reaction under oxic conditions was higher than that under anoxic conditions. Dissolved As mainly existed as As(III) under anoxic conditions. Dissolved S species mainly existed as SO_4^{2-} under anoxic conditions, which was different from the dominant S species of $S_2O_3^{2-}$ under oxic conditions. Under anoxic conditions, lower [As(T)], [As(III)], [As(V)], [$S_2O_3^{2-}$] and [SO_4^{2-}] were detected. Fig. 6 shows the instant [H_2O_2] and cumulative [·OH] in the above reaction processes. Under darkness and UV radiation, the maximum instant [H_2O_2] and cumulative [·OH] were lower under anoxic conditions than those under oxic conditions. The cumulative [·OH] and instant [H_2O_2] under UV radiation were higher and lower than those under darkness, respectively.

3.6. Influence of pH on As release and ROS production

The effect of pH on realgar oxidation and As release was investigated at pH 2.0 and 8.0 (Fig. 7). As(III) was still the primary form of dissolved As at different initial pH values. The dominant species of dissolved S was SO_4^{2-} at pH 2.0, while $S_2O_3^{2-}$ at pH 5.0 and 8.0. With increasing pH from 2.0 to 8.0, [As(T)], [As(III)], [As(V)], [S^{2-}], [$S_2O_3^{2-}$] and [SO_4^{2-}] increased under darkness and UV radiation. Fig. 8 shows the instant [H_2O_2] and cumulative [·OH] in the reaction at different initial pH values. Under darkness and UV radiation, the maximum instant [H_2O_2] and cumulative [·OH] increased with increasing pH. The cumulative [·OH] and instant [H_2O_2] under UV radiation also were higher and lower than those under darkness, respectively.

4. Discussion

4.1. Mechanism of realgar oxidation and As release under darkness

Under darkness, ROS contributed much to realgar oxidation and As release. ·OH and H_2O_2 were detected under darkness, and the As (T) release ratio decreased by 30.5%, 16.9% and 40.1% in the presence of BA, SOD and POD, respectively (Fig. 2), demonstrating that the ROS play an important role in realgar oxidation.

The loss of a S from S_2^{2-} may lead to the production of Fe(III) and sulfur-defect sites on pyrite (Borda et al., 2001). In anoxic environments, Fe(III) at sulfur-defect sites induces the decomposition of adsorbed H_2O into ·OH, and the combination of ·OH itself results in the generation of H_2O_2 (Zhang et al., 2016). In this work, the oxidative release of As and these ROS were detected in realgar suspension under anoxic conditions (Figs. 5 and 6). It can be speculated that ·OH and H_2O_2 might be formed through Eqs. (2) and (3):

$$As(III)_{vacancy} + H_2O \rightarrow As(II)_{vacancy} + {}^{\cdot}OH + H^+ \quad (2)$$

$$2\,{}^{\cdot}OH \rightarrow H_2O_2 \quad (3)$$

The XPS spectra indicated the presence of As(III)–S in initial realgar. In addition, realgar exhibited a strong EPR signal with a g-value of 2.003, indicating the presence of S vacancy (Fig. S4) (Bai et al., 2022; Wang et al., 2021a). After treatment with HCl solution (1.0 mol/L) for 12 h, the relative content of As(III) decreased from 7.3% to 1.7%, and the corresponding [H_2O_2], [·OH]

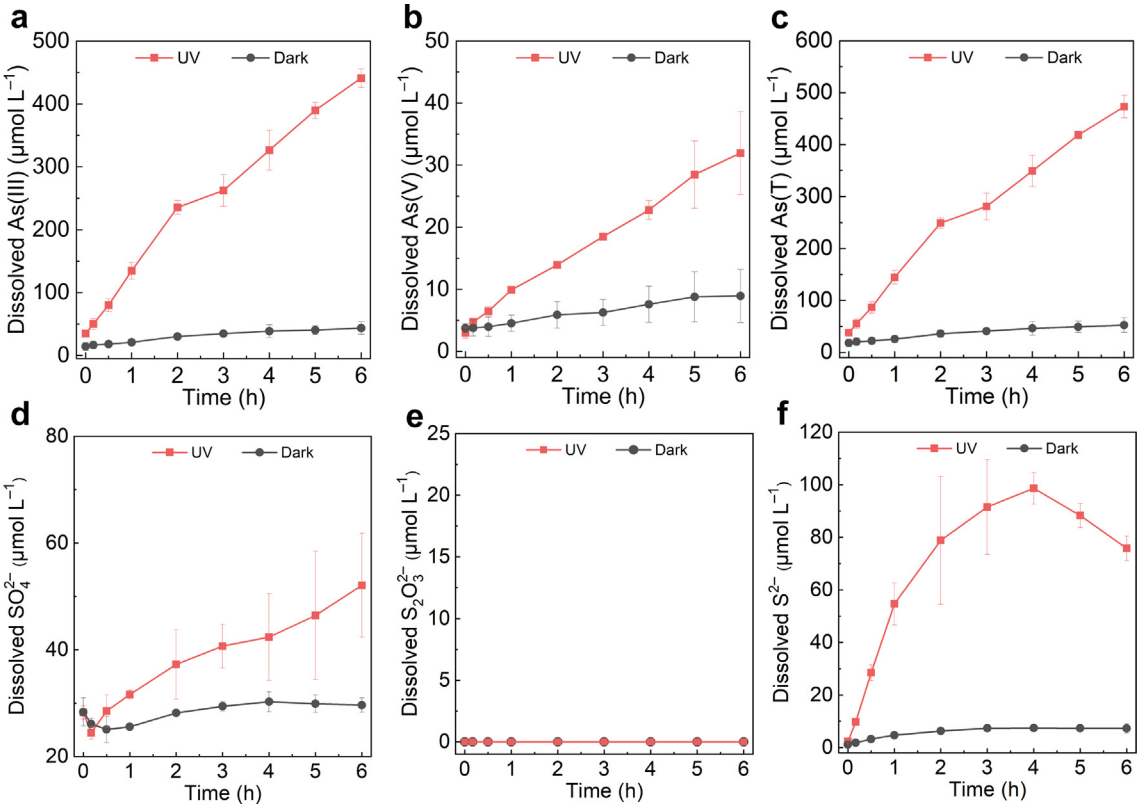

Fig. 5. Dissolved [As(III)] (a), [As(V)] (b), [As(T)] (c), [SO_4^{2-}] (d), [$S_2O_3^{2-}$] (e) and [S^{2-}] (f) in realgar suspension (0.5 g/L) under darkness and UV radiation at initial pH 5.0 and anoxic condition.

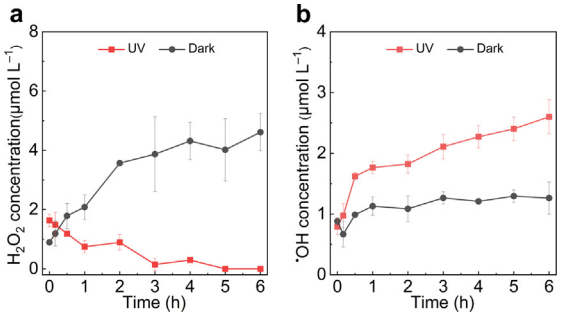

Fig. 6. Instant [H_2O_2] (a) and cumulative [·OH] (b) in realgar suspension (0.5 g/L) under darkness and UV radiation at initial pH 5.0 and anoxic condition.

and [As(T)] also significantly decreased (Fig. S5). With the continuous introduction of N_2 (99.99%), the initial [DO] was 0.7 mg/L, and [DO] decreased during the reaction, indicating the continuous consummation of DO. ROS may also be generated from the interaction between DO and As(II) on realgar ($As(II)_{realgar}$). The electronic configuration of $As(II)_{realgar}$ ($[Ar]3d^{10}4s^24p^1$) is unstable, and it is easy to reach the stable configuration of $As(III)_{realgar}$ by releasing an electron (Lengke and Tempel, 2003). Therefore, H_2O_2 may be generated from Eq. (4):

$$2As(II)_{realgar} + O_2 + 2H^+ \rightarrow 2As(III)_{realgar} + H_2O_2 \quad (4)$$

This process is similar to the production of ROS on pyrite in the oxidation of Fe(II) on pyrite by DO (Kong et al., 2015; Liu et al., 2021a; Zhang et al., 2016). Although the reaction between $As(II)_{realgar}$ and O_2 may also lead to the generation of $O_2^{\cdot-}$ (Kong et al., 2015; Liu et al., 2021a), no obvious signal of DMPO-$O_2^{\cdot-}$ was observed under darkness. Moreover, there was no obvious decrease in [As(T)] after the addition of SOD to the system. Therefore, H_2O decomposition at the sulfur-defect sites and the interaction between $As(II)_{realgar}$ and DO on realgar lead to the production of ROS and oxidation of realgar under darkness.

4.2. Mechanism of realgar oxidation and As release under UV radiation

UV light significantly promoted realgar oxidation and As release. It is widely known that light can induce the transformation of realgar solid to pararealgar solid in air, which is accompanied by the formation of As_2O_3 and elemental S. The reaction processes are shown as Eqs. (5) and (6) (Kyono et al., 2005; Naumov et al., 2010; Trentelman et al., 1996):

$$5As_4S_4(realgar) + 3O_2 + h\nu \rightarrow 4As_4S_5 + 2As_2O_3 \quad (5)$$

$$8As_4S_5 \rightarrow 8As_4S_4(pararealgar) + S_8 \quad (6)$$

In this work, it can be speculated that the photochemical transformation and As release processes of realgar in aqueous solution may occur as Eq. (7):

$$10As_4S_4(realgar) + 6O_2 + 12H_2O + h\nu \rightarrow 8As_4S_4(pararealgar) + S_8 + 8H_3AsO_3 \quad (7)$$

Although elemental S is a common product during the oxidation of realgar under darkness (Wang et al., 2022), the occurrence of the above reactions can be confirmed by the simultaneous existence of pararealgar and elemental S in the solid products (Fig. 3a). No As_4S_5 was found in the XRD patterns, which was likely due to its low chemical stability and crystallinity (Kyono et al., 2005).

Arsenic sulfides are usually semiconductor minerals. Previous studies have demonstrated that light-excited amorphous As_2S_3 and orpiment can generate h^+_{vb}–e^-_{cb} pairs (Lu et al., 2019). The h^+_{vb}

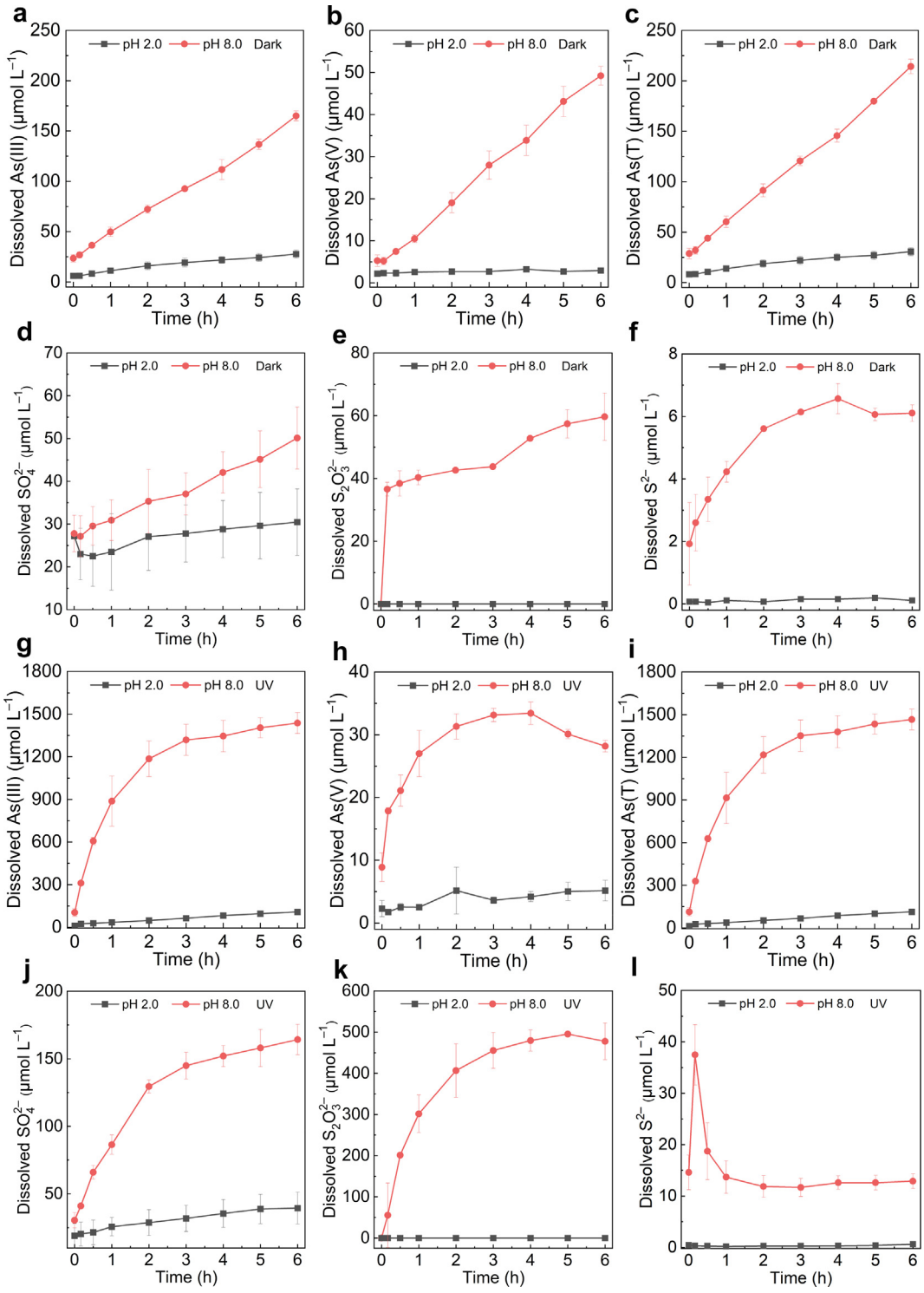

Fig. 7. Dissolved [As] and [S] in realgar suspension (0.5 g/L) under darkness (a–f) and UV radiation (g–l) at initial pH 2.0 and 8.0 and oxic condition.

can react with H_2O to form ·OH, and the e^-_{cb} can reduce DO to form $O_2^{\cdot-}$, which greatly contribute to the oxidative dissolution and As release of sulfide minerals (Lu et al., 2019). These processes were also found in our previous study about the photochemical oxidation of As-bearing iron sulfide minerals (Hong et al., 2018; Hong et al., 2020; Liu et al., 2021a). The band gap (Eg) of realgar was 2.07 eV, as measured through the relationship between the excitation wavelength (λ = 600 nm) and Eg of semiconductor (Eg = 1240/λ) (Fig. 9a) (Guo et al., 2018). The conduction band (CB) and VB potential can be calculated to be −0.38 V and 1.69 V (vs normal hydrogen electrode (NHE)) according to the Eg, XPS VB spectrum and Mott-Schottky plot (Fig. 9b and c, Table S1). The CB potential of realgar is lower than the reduction potential of O_2 to $O_2^{\cdot-}$ (−0.33 V vs NHE) and the VB potential is lower than the oxidation potential of H_2O to ·OH (2.38 V vs NHE) (Xu et al., 2021). Therefore, the e^-_{cb} can reduce O_2 to $O_2^{\cdot-}$ and the h^+_{vb} cannot oxidize H_2O to ·OH on realgar surface under light radiation (Fig. 9d). The higher [·OH] and lower [H_2O_2] under UV radiation than that under darkness can

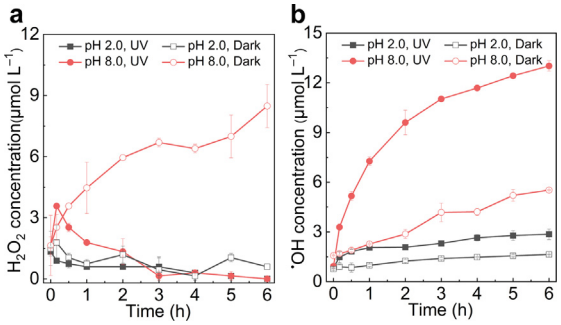

Fig. 8. Instant [H_2O_2] (a) and cumulative [·OH] (b) in realgar suspension (0.5 g/L) under darkness and UV radiation at initial pH 2.0 and 8.0 and oxic condition.

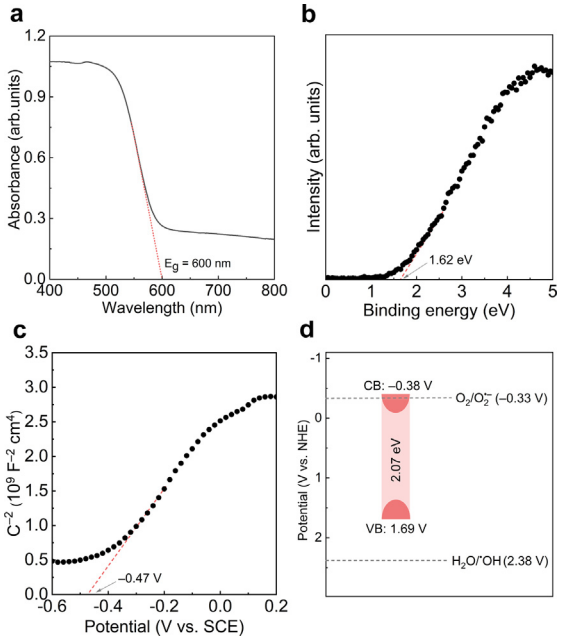

Fig. 9. UV–vis DRS (a), XPS VB spectrum (b), Mott-Schottky plot (c) and schematic illustration of the band structure (d) of realgar.

be attributed to the light-induced decomposition of H_2O_2 to ·OH (Hong et al., 2018). After the addition of BA and SOD to the reaction system, the [As(T)] decreased only by 25.4% and 16.6%, respectively (Fig. 2), suggesting that light-induced transformation of realgar to pararealgar instead of the formation of ROS contributes much to realgar oxidation and As release under UV radiation.

4.3. Speciation of released As during realgar oxidation

Although ROS can oxidize As(III) to As(V) (Liu et al., 2021a; Zeng et al., 2021), the [As(III)] was much higher than [As(V)] under darkness and UV radiation, which was further indicated by the experiment conducted for 48 h under anoxic conditions. After 48 h of reaction, [As(III)] and [As(V)] were 411.2 and 71.0 μmol/L under darkness, and 1574.8 and 30.7 μmol/L under UV radiation, respectively.

Under darkness, the formation of more As(III) than As(V) was also observed during the ROS-promoted oxidative dissolution of single As-bearing pyrite and arsenopyrite under anoxic conditions (Hong et al., 2018; Hong et al., 2020; Zhang et al., 2017). During these reactions, ROS were mainly generated on the mineral surface (Hong et al., 2018; Hong et al., 2020; Zhang et al., 2017). Similarly, our results indicated that the realgar oxidation and the subsequent As release were also mainly attributed to the generation of H_2O_2 and ·OH on realgar surface. At pH < 9, As mainly exists as uncharged H_3AsO_3 (Liu et al., 2021b). As reported, H_2O_2 is difficult to oxidize undissociated As(III) to As(V) (Wang et al., 2021b). In addition, the lifetime of radicals is very short (10^{-12}–10^{-6} s) in solutions, and thus the reaction of radicals associated with mineral surface mainly occur at or close to the formation site (Xu et al., 2013). Therefore, ROS may preferentially oxidize As(II) on realgar surface instead of As(III) in the solution, which led to the formation of more As(III) in solution.

Despite that the As(T) release ratio significantly increased under UV and solar radiation, the [As(V)] was lower than that under darkness. The rapid transformation of realgar to pararealgar under light radiation was mainly accompanied by the release of As(III); while the formation of ROS contributed more to realgar oxidation and As release under darkness, which can promote the oxidation of a part of As(III) to As(V) (Liu et al., 2021a; Zeng et al., 2021). The differences in the oxidation mechanism led to the lower [As(V)] under UV radiation than that under darkness.

4.4. Influencing factors of As release

More As was released under oxic conditions than under anoxic conditions. DO was consumed in the reaction process (Fig. S3). Realgar oxidation and As release were mainly promoted by ROS, and more H_2O_2 and ·OH were generated under oxic conditions under darkness (Figs. 2 and 6). Under UV radiation, the transformation of realgar to pararealgar and ROS generated on the light-excited realgar together enhanced As release. The transformation of realgar to pararealgar depends on the [DO] (Eq. (7)), and a higher [DO] would lead to a faster transformation rate. In addition, during the formation of ROS through h^+_{vb}–e^-_{cb} pairs on light-excited realgar, the higher [DO] could directly promote the formation of more $O_2^{\cdot-}$ (Liu et al., 2021a). Therefore, As release rate was higher under oxic conditions. Under both darkness and UV radiation, dissolved S mainly existed as SO_4^{2-} under anoxic conditions, while as $S_2O_3^{2-}$ under oxic conditions (Figs. 1 and 5). ROS, which have obviously stronger oxidation activities than DO, acted as the dominant oxidant to mainly oxidize S^{2-} to SO_4^{2-} under anoxic conditions (Hong et al., 2021). DO can oxidize a part of S^{2-} first to $S_2O_3^{2-}$ and then to SO_4^{2-} at mineral surface (Kleinjan et al., 2005), which can explain the increase in the proportion of SO_4^{2-} under anoxic conditions compared with under oxic conditions.

The rate of realgar oxidation and As(T) release was accelerated with increasing pH from 2.0 to 8.0. Under darkness, an increase in pH can accelerate the decomposition of H_2O to ROS at the sulfur-defect sites (Eq. (2)), thereby promoting the release of As. Under UV radiation, the transformation of realgar to pararealgar and further oxidation of As(III) to As(V) or elemental S to oxysulfide anions were accompanied by the formation of H^+ (Eq. (7) and Fig. S6) (Lengke and Tempel, 2003; Zhao et al., 2017), and an increase in pH was conducive to the transformation of realgar to pararealgar. In addition, although no As_2S_3 was observed in the XRD patterns (Fig. S7), the precipitation of amorphous As_2S_3 may also contribute to the lower [As(T)] in solution at a low pH, which exists as a very common precipitate under high arsenic, sulfide and proton activities (Ferguson and Gavis, 1972; Ostermeyer et al., 2021). The higher Eh could not cause the oxidation of more realgar at pH 2.0 (Fig. S8), which was also found in the previous work (Lengke and Tempel, 2003; Lengke and Tempel, 2005). This phenomenon can be explained by the fact that pH and DO are more important factors affecting realgar oxidation compared with Eh (Lengke and Tempel, 2005). The increase in ROS content was also conducive to the formation of SO_4^{2-}. Dissolved S mainly existed as SO_4^{2-} at pH 2.0, while as $S_2O_3^{2-}$ at pH 5.0 and 8.0, which may be ascribed

to the decomposition of $S_2O_3^{2-}$ to S, SO_2 and H_2O at pH 2.0 (Kong et al., 2020).

4.5. Environmental significance

Under darkness, realgar can induce ROS formation in the system with low [DO]. The shallow groundwater system is a typical environment generally with [DO] lower than 5.0 mg/L (Burow et al., 2010; Thayalakumaran et al., 2008). Species of As in aquifer sediments and pore waters are a key factor determining the potential toxicity of dissolved As (O'Day et al., 2004). The microbial-mediated reduction of As-bearing iron oxides is generally known as an important factor causing As pollution in groundwaters (Kirk et al., 2010; Li et al., 2022; Podgorski and Berg, 2020). Numerous studies have shown that realgar is also one of the important As-bearing sulfide minerals in anoxic shallow aquifer sediments and As-rich wetlands, and its formation is accompanied by As concentration attenuation in these environments (Drahota et al., 2017; Gallegos et al., 2008; Knappová et al., 2019; O'Day et al., 2004). However, realgar also may be oxidized and dissolved when [DO] increases due to seasonal water table level fluctuations (Wang et al., 2022). The results of the present study indicate that decomposition of H_2O at sulfur-defect sites of realgar to form ROS in the presence of [DO] may result in As pollution in groundwaters. In the soil and water around the mine, oxidation of As-bearing minerals is an important source of As pollution (Liu et al., 2021a; Tang et al., 2017). During the mining and smelting of precious metals such as gold, silver and lead, the associated realgar is easy to be exposed to air and H_2O in tailings (Bullen et al., 2003). Our results confirm that the existence of DO accelerates the formation of ROS under oxic conditions, and then promotes realgar oxidative dissolution and As release.

Although the potential toxic impact of mining dust and wastewater have been known, many abandoned realgar-bearing tailings and slags are still exposed to solar radiation and air without cover due to a lack of appropriate management (Đorđević et al., 2019; Kerr et al., 2018; Li et al., 2020; Wang et al., 2019). A number of studies have shown that sunlight significantly affects the physicochemical properties of semiconductor minerals in the environment, especially sulfide minerals and oxide minerals (Hu et al., 2015; Kong et al., 2018). Under solar radiation, the ROS produced on these excited semiconductor minerals through $h^+_{vb}-e^-_{cb}$ pairs can significantly affect the species and migration of toxic elements (Hong et al., 2021; Kong et al., 2015; Liu et al., 2022a; Lu et al., 2019). Recently, a study showed that in the streams around Shimen realgar mining area in Hunan Province, China, the As concentration in summer was significantly higher than that in winter, which was mainly ascribed to the effect of microbial activity and temperature (Li et al., 2020). The results of this work indicate that the seasonal variation of As pollution could also be related to more sunlight exposure of realgar in summer. Previous studies have demonstrated that the formation of ·OH and $O_2^{\cdot-}$ on light-excited amorphous arsenic sulfide (As_2S_3) in sludge is a key reason for As release (Lu et al., 2019), which significantly differs from the As release mechanism of realgar. Light-induced oxidation of realgar to pararealgar in the presence of DO was proved to be the main reason for the accelerated release of As. Although the UV light intensity in UV lamp was about 6.8-fold that in sunlight, the As release ratio in sunlit system (18.1%) was close to that in the system under UV radiation (17.0%) and about 4.3-fold that in the system under darkness (Fig. S9), which can be ascribed to the high intensity of visible light in solar radiation. These results further demonstrated that solar radiation may be an important environmental factor causing As pollution in waters and soils around realgar mining areas. However, in complicated and variable realistic tailings environment, some other minerals including pyrite, arsenopyrite, orpiment and stibnite commonly coexist with realgar. These minerals exhibit photochemical properties or adsorption/(catalytic) oxidation ability for As, and thereby may significantly affect realgar oxidation and As migration (Đorđević et al., 2019; Hong et al., 2021; Kerr et al., 2018). Therefore, further investigations about the effect of solar radiation on realgar oxidation are needed in realistic tailings.

The oxidation of sulfide minerals can lead to the generation of acid mine drainage (AMD) with low pH to 2.0 (Kerr et al., 2018; Kong et al., 2020; Zhang et al., 2016). During the treatment of AMD with simple chemical neutralization, the increase in pH can cause the formation of more ROS on realgar, which is the essential reason for the enhanced realgar oxidative dissolution and As release in neutral and weakly alkaline environments (Fig. 7). Realgar is a sulfide mineral without stoichiometric iron, and the released As species is mainly As(III). Iron oxides have a high affinity for As(V) (Dixit and Hering, 2003). Iron-bearing amendments including ferrous salts and zero valent iron can produce ROS in their oxidation by DO and promote the further oxidation of As (III) to As(V) (Wang et al., 2019; Zhao et al., 2020). Therefore, the application of these iron-bearing amendments can decrease As mobility and toxicity in the contaminated area of realgar tailings.

5. Conclusions

The exposure of realgar to DO and solar radiation promotes its oxidation and As release. The released As species in solutions mainly existed as As(III), particularly under solar radiation. Under darkness, the decomposition of H_2O at the sulfur-defect sites and the oxidation of As(II) by DO on realgar surface led to the formation of ·OH and H_2O_2, resulting in the oxidative dissolution of realgar and As release. Under solar radiation, the reaction between O_2 and e^-_{cb} caused the production of more $O_2^{\cdot-}$, while the accelerated realgar oxidation and As release rate were mainly attributed to the light-induced oxidation of realgar to pararealgar in the presence of DO. The higher DO concentration and pH led to the increase in realgar oxidation and As release. Therefore, in addition to DO, solar radiation may also be an important environmental factor causing As pollution in waters and soils in realgar mining areas. The present work improves the understanding of realgar oxidation and As release in groundwaters and surface mining environments of realgar tailings.

Declaration of Competing Interest

The authors declare that they have no known competing financial interests or personal relationships that could have appeared to influence the work reported in this paper.

Data availability

Data will be made available on request.

Acknowledgments

This work was supported by the National Natural Science Foundation of China (41877025 and 42077133), the National Key Research & Development Program of China (2020YFC1808503), HZAU-AGIS Cooperation Fund (SZYJY2022035), Leading Talent of "Ten Thousand Plan"-National High-Level Talents Special Support Plan, West Light Foundation and the Frontier Science Research Programme of the Chinese Academy of Sciences (QYZDB-SSW-DQC046).

Appendix A. Supplementary material

Supplementary material to this article can be found online at https://doi.org/10.1016/j.gca.2022.10.037.

References

Bai, X., Wang, X., Jia, T., Guo, L., Hao, D., Zhang, Z., Wu, L., Zhang, X., Yang, H., Gong, Y., 2022. Efficient degradation of PPCPs by $Mo_{1-x}S_{2-y}$ with S vacancy at phase-junction: Promoted by innergenerate-H_2O_2. Appl. Catal. B 310, 121302.

Borda, M.J., Elsetinow, A.R., Schoonen, M.A., Strongin, D.R., 2001. Pyrite-induced hydrogen peroxide formation as a driving force in the evolution of photosynthetic organisms on an early Earth. Astrobiology 1, 283–288.

Bullen, H.A., Dorko, M.J., Oman, J.K., Garrett, S.J., 2003. Valence and core-level binding energy shifts in realgar (As_4S_4) and pararealgar (As_4S_4) arsenic sulfides. Surf. Sci. 531, 319–328.

Burow, K.R., Nolan, B.T., Rupert, M.G., Dubrovsky, N.M., 2010. Nitrate in groundwater of the United States, 1991–2003. Environ. Sci. Technol. 44, 4988–4997.

Chen, P., Yan, L., Wang, Q., Li, H., 2013. Arsenic precipitation in the bioleaching of realgar using *acidithiobacillus ferrooxidans*. J. Appl. Chem. 2013, 1–5.

Dixit, S., Hering, J.G., 2003. Comparison of arsenic(V) and arsenic(III) sorption onto iron oxide minerals: Implications for arsenic mobility. Environ. Sci. Technol. 37, 4182–4189.

Doane, T.A., 2017. A survey of photogeochemistry. Geochem. Trans. 18, 1–24.

Dong, G., Huang, Y., Yu, Q., Wang, Y., Wang, H., He, N., Li, Q., 2014. Role of nanoparticles in controlling arsenic mobilization from sediments near a realgar tailing. Environ. Sci. Technol. 48, 7469–7476.

Đorđević, T., Kolitsch, U., Serafimovski, T., Tasev, G., Tepe, N., Stöger-Pollach, M., Hofmann, T., Boev, B., 2019. Mineralogy and weathering of realgar-rich tailings at a former As-Sb-Cr mine at Lojane, North Macedonia. Can. Mineral. 57, 403–423.

Drahota, P., Mikutta, C., Falteisek, L., Duchoslav, V., Klementová, M., 2017. Biologically induced formation of realgar deposits in soil. Geochim. Cosmochim. Acta 218, 237–256.

Falteisek, L., Drahota, P., Culka, A., Laufek, F., Trubač, J., 2020. Bioprecipitation of As_4S_4 polymorphs in an abandoned mine adit. Appl. Geochem. 113, 104511.

Fan, L., Zhao, F., Liu, J., Hudson-Edwards, K.A., 2018. Dissolution of realgar by *Acidithiobacillus ferrooxidans* in the presence and absence of zerovalent iron: Implications for remediation of iron-deficient realgar tailings. Chemosphere 209, 381–391.

Ferguson, J.F., Gavis, J., 1972. A review of the arsenic cycle in natural waters. Water Res. 6, 1259–1274.

Gallegos, T.J., Han, Y.S., Hayes, K.F., 2008. Model predictions of realgar precipitation by reaction of As(III) with synthetic mackinawite under anoxic conditions. Environ. Sci. Technol. 42, 9338–9343.

Guo, J.-G., Liu, Y., Hao, Y.-J., Li, Y.-L., Wang, X.-J., Liu, R.-H., Li, F.-T., 2018. Comparison of importance between separation efficiency and valence band position: The case of heterostructured Bi_3O_4Br/α-Bi_2O_3 photocatalysts. Appl. Catal. B 224, 841–853.

Hong, J., Liu, L., Luo, Y., Tan, W., Qiu, G., Liu, F., 2018. Photochemical oxidation and dissolution of arsenopyrite in acidic solutions. Geochim. Cosmochim. Acta 239, 173–185.

Hong, J., Liu, L., Tan, W., Qiu, G., 2020. Arsenic release from arsenopyrite oxidative dissolution in the presence of citrate under UV irradiation. Sci. Total. Environ. 726, 138429.

Hong, J., Liu, L., Ning, Z., Liu, C., Qiu, G., 2021. Synergistic oxidation of dissolved As (III) and arsenopyrite in the presence of oxygen: Formation and function of reactive oxygen species. Water Res. 202, 117416.

Hong, J., Liu, L., Zhang, Z., Xia, X., Yang, L., Ning, Z., Liu, C., Qiu, G., 2022. Sulfate-accelerated photochemical oxidation of arsenopyrite in acidic systems under oxic conditions: Formation and function of schwertmannite. J. Hazard. Mater. 433, 128716.

Hu, X., He, M., Kong, L., 2015. Photopromoted oxidative dissolution of stibnite. Appl. Geochem. 61, 53–61.

Hu, S., Lu, J., Jing, C., 2012. A novel colorimetric method for field arsenic speciation analysis. J. Environ. Sci. 24, 1341–1346.

Ilton, E.S., Post, J.E., Heaney, P.J., Ling, F.T., Kerisit, S.N., 2016. XPS determination of Mn oxidation states in Mn (hydr)oxides. Appl. Surf. Sci. 366, 475–485.

Kerr, G., Craw, D., Trumm, D., Pope, J., 2018. Authigenic realgar and gold in dynamic redox gradients developed on historic mine wastes, New Zealand. Appl. Geochem. 97, 123–133.

Kirk, M.F., Roden, E.E., Crossey, L.J., Brealey, A.J., Spilde, M.N., 2010. Experimental analysis of arsenic precipitation during microbial sulfate and iron reduction in model aquifer sediment reactors. Geochim. Cosmochim. Acta 74, 2538–2555.

Kleinjan, W.E., de Keizer, A., Janssen, A.J., 2005. Kinetics of the chemical oxidation of polysulfide anions in aqueous solution. Water Res. 39, 4093–4100.

Knappová, M., Drahota, P., Falteisek, L., Culka, A., Penížek, V., Trubač, J., Mihaljevič, M., Matoušek, T., 2019. Microbial sulfidogenesis of arsenic in naturally contaminated wetland soil. Geochim. Cosmochim. Acta 267, 33–50.

Kong, L., Hu, X., He, M., 2015. Mechanisms of Sb(III) oxidation by pyrite-induced hydroxyl radicals and hydrogen peroxide. Environ. Sci. Technol. 49, 3499–3505.

Kong, L., Peng, X., Hu, X., Chen, J., Xia, Z., 2018. UV-light-induced aggregation of arsenic and metal sulfide particles in acidic wastewater: The role of free radicals. Environ. Sci. Technol. 52, 10719–10727.

Kong, L., Hu, X., Peng, X., Wang, X., 2020. Specific H_2S release from thiosulfate promoted by UV irradiation for removal of arsenic and heavy metals from strongly acidic wastewater. Environ. Sci. Technol. 54, 14076–14084.

Kyono, A., Kimata, M., Hatta, T., 2005. Light-induced degradation dynamics in realgar: In situ structural investigation using single-crystal X-ray diffraction study and X-ray photoelectron spectroscopy. Am. Mineral. 90, 1563–1570.

Langner, P., Mikutta, C., Kretzschmar, R., 2014. Oxidation of organosulfur-coordinated arsenic and realgar in peat: Implications for the fate of arsenic. Environ. Sci. Technol. 48, 2281–2289.

Lázaro, I., González, I., Cruz, R., Monroy, M.G., 1997. Electrochemical study of orpiment (As_2S_3) and realgar (As_2S_2) in acidic medium. J. Electrochem. Soc. 144, 4128–4132.

Lengke, M.F., Tempel, R.N., 2003. Natural realgar and amorphous AsS oxidation kinetics. Geochim. Cosmochim. Acta 67, 859–871.

Lengke, M.F., Tempel, R.N., 2005. Geochemical modeling of arsenic sulfide oxidation kinetics in a mining environment. Geochim. Cosmochim. Acta 69, 341–356.

Lengke, M.F., Sanpawanitchakit, C., Tempel, R.N., 2009. The oxidation and dissolution of arsenic-bearing sulfides. Can. Mineral. 47, 593–613.

Lenoble, V., 2003. Arsenite oxidation and arsenate determination by the molybdene blue method. Talanta 61, 267–276.

Li, H., Zeng, X.C., He, Z., Chen, X., Guoji, E., Han, Y., Wang, Y., 2016. Long-term performance of rapid oxidation of arsenite in simulated groundwater using a population of arsenite-oxidizing microorganisms in a bioreactor. Water Res. 101, 393–401.

Li, W., Liu, J., Hudson-Edwards, K.A., 2020. Seasonal variations in arsenic mobility and bacterial diversity: The case study of Huangshui Creek, Shimen Realgar Mine, Hunan Province. China. Sci. Total. Environ. 749, 142353.

Li, Y., Yu, C., Zhao, B., Chen, D., Ye, H., Nagel, C., Shao, W., Oelmann, Y., Neidhardt, H., Guo, H., 2022. Spatial variation in dissolved phosphorus and interactions with arsenic in response to changing redox conditions in floodplain aquifers of the Hetao Basin. Inner Mongolia. Water Res. 209, 117930.

Liu, L., Jia, Z., Tan, W., Suib, S.L., Ge, L., Qiu, G., Hu, R., 2018. Abiotic photomineralization and transformation of iron oxide nanominerals in aqueous systems. Environ. Sci.: Nano 5, 1169–1178.

Liu, L., Guo, D., Ning, Z., Liu, C., Qiu, G., 2021a. Solar irradiation induced oxidation and adsorption of arsenite on natural pyrite. Water Res. 203, 117545.

Liu, L., Qiao, Q., Tan, W., Sun, X., Liu, C., Dang, Z., Qiu, G., 2021b. Arsenic detoxification by iron-manganese nodules under electrochemically controlled redox: Mechanism and application. J. Hazard. Mater. 403, 123912.

Liu, L., Guo, D., Qiu, G., Liu, C., Ning, Z., 2022a. Photooxidation of Fe(II) to schwertmannite promotes As(III) oxidation and immobilization on pyrite under acidic conditions. J. Environ. Manage. 317, 115425.

Liu, L., Li, A., Cao, M., Ma, J., Tan, W., Suib, S.L., Qiu, G., 2022b. Photoinduced self-organized precipitation in leachate for remediation of heavy metal contaminated soils. ACS EST Engg. 2, 1376–1385.

Lu, H., Liu, X., Liu, F., Hao, Z., Zhang, J., Lin, Z., Barnett, Y., Pan, G., 2019. Visible-light photocatalysis accelerates As(III) release and oxidation from arsenic-containing sludge. Appl. Catal. B 250, 1–9.

Naidu, G., Ryu, S., Thiruvenkatachari, R., Choi, Y., Jeong, S., Vigneswaran, S., 2019. A critical review on remediation, reuse, and resource recovery from acid mine drainage. Environ. Pollut. 247, 1110–1124.

Najafi, A., Hashemi, M., 2019. Vortex-assisted supramolecular solvent microextraction based on solidification of floating drop for preconcentration and speciation of inorganic arsenic species in water samples by molybdenum blue method. Microchem. J. 150, 104102.

Naumov, P., Makreski, P., Petrusevski, G., Runcevski, T., Jovanovski, G., 2010. Visualization of a discrete solid-state process with steady-state X-ray diffraction: Observation of hopping of sulfur atoms in single crystals of realgar. J. Am. Chem. Soc. 132, 11398–11401.

O'Day, P.A., Vlassopoulos, D., Root, R., Rivera, N., 2004. The influence of sulfur and iron on dissolved arsenic concentrations in the shallow subsurface under changing redox conditions. Proc. Natl. Acad. Sci. U.S.A. 101, 13703–13708.

Oscarson, D.W., Huang, P.M., Liaw, W.K., 1980. The oxidation of arsenite by aquatic sediments. J. Environ. Qual. 9, 700–703.

Ostermeyer, P., Bonin, L., Folens, K., Verbruggen, F., Garcia-Timermans, C., Verbeken, K., Rabaey, K., Hennebel, T., 2021. Effect of speciation and composition on the kinetics and precipitation of arsenic sulfide from industrial metallurgical wastewater. J. Hazard. Mater. 409, 124418.

Podgorski, J., Berg, M., 2020. Global threat of arsenic in groundwater. Science 368, 845–850.

Qiu, G., Gao, T., Hong, J., Tan, W., Liu, F., Zheng, L., 2017. Mechanisms of arsenic-containing pyrite oxidation by aqueous arsenate under anoxic conditions. Geochim. Cosmochim. Acta 217, 306–319.

Qiu, G., Gao, T., Hong, J., Luo, Y., Liu, L., Tan, W., Liu, F., 2018. Mechanisms of interaction between arsenian pyrite and aqueous arsenite under anoxic and oxic conditions. Geochim. Cosmochim. Acta 228, 205–219.

Renock, D., Becker, U., 2010. A first principles study of the oxidation energetics and kinetics of realgar. Geochim. Cosmochim. Acta 74, 4266–4284.

Rodriguez-Lado, L., Sun, G., Berg, M., Zhang, Q., Xue, H., Zheng, Q., Johnson, C.A., 2013. Groundwater arsenic contamination throughout China. Science 341, 866–868.

Shu, Z., Liu, L., Tan, W., Suib, S.L., Qiu, G., Yang, X., Zheng, L., Liu, F., 2019. Solar irradiation induced transformation of ferrihydrite in the presence of aqueous Fe^{2+}. Environ. Sci. Technol. 53, 8854–8861.

Tang, L., Feng, H., Tang, J., Zeng, G., Deng, Y., Wang, J., Liu, Y., Zhou, Y., 2017. Treatment of arsenic in acid wastewater and river sediment by $Fe@Fe_2O_3$

nanobunches: The effect of environmental conditions and reaction mechanism. Water Res. 117, 175–186.
Thayalakumaran, T., Bristow, K.L., Charlesworth, P.B., Fass, T., 2008. Geochemical conditions in groundwater systems: Implications for the attenuation of agricultural nitrate. Agric. Water Manage. 95, 103–115.
Trentelman, K., Stodulski, L., Pavlosky, M., 1996. Characterization of pararealgar and other light-induced transformation products from realgar by Raman microspectroscopy. Anal. Chem. 68, 1755–1761.
Wang, J., Bo, T., Shao, B., Zhang, Y., Jia, L., Tan, X., Zhou, W., Yu, T., 2021a. Effect of S vacancy in Cu_3SnS_4 on high selectivity and activity of photocatalytic CO_2 reduction. Appl. Catal., B 297, 120498.
Wang, H.Y., Byrne, J.M., Perez, J.P.H., Thomas, A.N., Göttlicher, J., Höfer, H.E., Mayanna, S., Kontny, A., Kappler, A., Guo, H.M., Benning, L.G., Norra, S., 2020. Arsenic sequestration in pyrite and greigite in the buried peat of As-contaminated aquifers. Geochim. Cosmochim. Acta 284, 107–119.
Wang, Z., Fu, Y., Wang, L., 2021b. Abiotic oxidation of arsenite in natural and engineered systems: Mechanisms and related controversies over the last two decades (1999–2020). J. Hazard. Mater. 414, 125488.
Wang, X., Zhang, H., Wang, L., Chen, J., Xu, S., Hou, H., Shi, Y., Zhang, J., Ma, M., Tsang, D.C.W., Crittenden, J.C., 2019. Transformation of arsenic during realgar tailings stabilization using ferrous sulfate in a pilot-scale treatment. Sci. Total. Environ. 668, 32–39.
Wang, X., Wang, J., Lu, X., Zhou, M., Wang, Q., Pan, Z., Kumar, N., Zhu, M., Wang, Z., 2022. Oxidative dissolution of orpiment and realgar induced by dissolved and solid Mn(III) species. Geochim. Cosmochim. Acta 332, 307–326.
Wu, Y., Zhou, X.-Y., Lei, M., Yang, J., Ma, J., Qiao, P.-W., Chen, T.-B., 2017. Migration and transformation of arsenic: Contamination control and remediation in realgar mining areas. Appl. Geochem. 77, 44–51.
Xu, J., Sahai, N., Eggleston, C.M., Schoonen, M.A.A., 2013. Reactive oxygen species at the oxide/water interface: Formation mechanisms and implications for prebiotic chemistry and the origin of life. Earth Planet. Sci. Lett. 363, 156–167.
Xu, X., Wang, J., Chen, T., Yang, N., Wang, S., Ding, X., Chen, H., 2021. Deep insight into ROS mediated direct and hydroxylated dichlorination process for efficient photocatalytic sodium pentachlorophenate mineralization. Appl. Catal., B 296, 120352.
Yu, Y., Zhu, Y., Gao, Z., Gammons, C.H., Li, D., 2007. Rates of arsenopyrite oxidation by oxygen and Fe(III) at pH 1.8−12.6 and 15–45 °C. Environ. Sci. Technol. 41, 6460–6464.
Zeng, Y., Fang, G., Fu, Q., Dionysiou, D.D., Wang, X., Gao, J., Zhou, D., Wang, Y., 2021. Photochemical characterization of paddy water during rice cultivation: Formation of reactive intermediates for As(III) oxidation. Water Res. 206, 117721.
Zhang, P., Yuan, S., Liao, P., 2016. Mechanisms of hydroxyl radical production from abiotic oxidation of pyrite under acidic conditions. Geochim. Cosmochim. Acta 172, 444–457.
Zhang, P., Yao, W., Yuan, S., 2017. Citrate-enhanced release of arsenic during pyrite oxidation at circumneutral conditions. Water Res. 109, 245–252.
Zhao, C., Gupta, V.V., Degryse, F., McLaughlin, M.J., 2017. Effects of pH and ionic strength on elemental sulphur oxidation in soil. Biol. Fertil. Soils 53, 247–256.
Zhao, Z., Zhang, H., Wang, X., Yao, D., Hou, H., Shi, Y., Chen, J., Wang, L., Ma, M., Liu, J., Crittenden, J.C., 2020. The mechanism of microwave-induced mineral transformation and stabilization of arsenic in realgar tailings using ferrous sulfate. Chem. Eng. J. 393, 124732.